ACS APPLIED MATERIALS & INTERFACES

Research Article

www.acsami.org

Efficient Copper Mediators Based on Bulky Asymmetric Phenanthrolines for DSSCs

Alessia Colombo,*[,†] Claudia Dragonetti,[†] Mirko Magni,*[,†] Dominique Roberto,[†] Francesco Demartin,[†] Stefano Caramori,*[,‡] and Carlo A. Bignozzi[‡]

[†]Dipartimento di Chimica, Università degli Studi di Milano, UdR dell'INSTM, Via Golgi 19, Milano 20133 Italy

[‡]Dipartimento di Scienze Chimiche e Farmaceutiche, Università degli Studi di Ferrara, Via Fossato di Mortara 17, Ferrara 44121, Italy

Supporting Information

ABSTRACT: In the context of the development of new electron mediators for dye-sensitized solar cells that could efficiently substitute the more common I_3^-/I^- redox couple, we have prepared a series of Cu(I)- phenanthroline complexes through an easy synthetic route. The novel [Cu(2-mesityl-4,7-dimethyl-1,10-phenanthroline)$_2$]PF_6 (**3**) is of particular interest because the presence of the bulky mesityl groups protects as a kiss lock the Cu center, leading to superior dye regeneration kinetics with respect to simpler phenanthroline-based Cu(I) complexes and to a lower dark current with respect the I_3^-/I^-. The exploitation of a dual-component electrolyte constituted by (**3**) and a Fe(II) comediator, in combination with the [Ru(4,4′-dicarboxy-2,2′-bipyridine)$_2$(4,4′-dinonyl-2,2′-bipyridine)]$(PF_6)_2$ sensitizer, allowed us to increase the performance of the cell, reaching J_{sc} values of 4.0 mA cm^{-2}, comparable to that recorded with I_3^-/I^- (3.8 mA cm^{-2}).

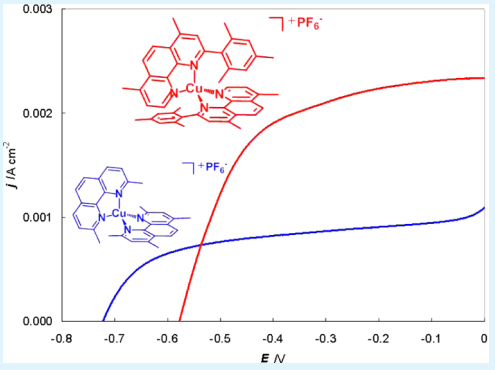

KEYWORDS: *copper electron mediators, cyclovoltammetry, DSSC*

1. INTRODUCTION

Dye-sensitized solar cells (DSSCs)[1−9] are considered a promising realistic solution for harnessing the energy of the sun and converting it into electrical energy, with power conversion efficiencies now exceeding the value of 12%.[10]

The basic elements of a DSSC are the photoanode (a layer of a nanocrystalline and mesoporous large band gap semiconductor such as TiO_2, which is sensitized by dye molecules), the cathode (usually composed of Pt nanoparticles), both of them dispersed on a glass covered with a thin layer of a transparent conductive oxide (usually a fluorinated tin oxide, FTO), and the electrolytic solution. The general mechanisms for light-to-electrical power conversion in DSSCs are the following: (i) light is absorbed by the sensitizer to form a molecular excited state; (ii) the excited state may inject an electron into the semiconductor thus causing charge separation; (iii) the oxidized sensitizer is "regenerated" by an external electron donor (a redox active electrolyte, as electron mediator). Once the electron has performed useful work in the external circuit, it returns to a counter electrode where it reduces the oxidized electron mediator.

In DSSCs, the electron mediator, which has a key role,[9] must simultaneously fulfill at least three strict requirements: it has to intercept efficiently the oxidized form of the dye, recombine slowly with photoinjected electrons on both TiO_2 and FTO substrates and allow for an efficient mass transport in solution and into the TiO_2 mesopores. The traditional redox couple is I_3^-/I^- because it has ideal kinetic properties: the forward electron donation by I^- is a facile monoelectronic process which ensures an efficient dye recovery, while the reduction of I_3^- appears to be largely inefficient allowing for a minimization of the interfacial back recombination. However, the I_3^-/I^- redox couple has some disadvantages: (i) I_2 in equilibrium with I_3^- is volatile, complicating long-term cell sealing; (ii) I_3^- is darkly colored and limits the light harvesting efficiency of the dye, (iii) DSSC cathodes require platinum coatings to obtain the best catalysis of I_3^- reduction at the counter electrode which also exhibits instability issues, (iv) large photovoltage loss due to the nonoptimal matching with the dye redox potential and (v) I_3^-/I^- is corrosive and will corrode most metals, posing a serious problem for the use of metal grid collectors necessary for scaling up the solar cells to large areas. Because of all these limitations, in recent years, there has been a lot of interest in the search for new electron transfer mediators, in particular based on transition metal complexes, the electrochemical properties of which can be easily tuned through a rational choice of the metal and an appropriate design of the coordination sphere.[9] To date, Co(II)/(III) polypyridine complexes represent the most successful examples of electron transfer mediators based on coordination compounds thanks to a combination of favorable optical and electrochemical properties, which since their first reports, however, required more than

Received: May 28, 2014
Accepted: July 31, 2014
Published: July 31, 2014

10 years of optimization of both dye design and electrode materials to be fully exploited[9] finally leading to record performances, such as the 12.5% efficiency reached in combination with a bulky Zn(II) porphyrin as sensitizer[10]

In this context, particularly appealing are copper complexes, already known as a useful dye-sensitizer component in DSSCs,[11−15] which recently proved to be promising efficient electron mediators for solar cells.[16,17] Under this respect, copper(I) mediators are much less studied respect to analogue Co(II) complexes with regard to the elementary heterogeneous electron transfer kinetics and interaction with selected dyes, therefore their kinetic and thermodynamic limitations have not been unambiguously identified. Cu(I)/(II) couples are usually characterized by slow electron transfer kinetics, due to a significant change in the preferred coordination geometry from tetrahedral Cu(I) to tetragonal Cu(II), that could guarantee inefficient electron recapture processes. However, if the electron transfer is too slow, a low efficiency in dye regeneration is expected and in order to optimize the electron transfer properties of the redox shuttles, the coordination sphere of the copper complex has to be rationally designed. Thus, in nature, it is known that copper systems such as "copper blue proteins" act as efficient electron transfer mediators because they have tetrahedrally distorted geometries intermediate between Cu(I) and Cu(II) ones, so the geometry of the active site is optimized for a fast electron transfer.[18−22] The use of copper complexes with a distorted tetragonal geometry, in which the structural change between the Cu(I) and Cu(II) complexes is minimized, clearly provides a promising strategy to electron mediators for DSSCs, because they allow a very fast electron transfer and a redox potential of the Cu(I)/Cu(II) couple high enough to increase V_{oc} values.[16]

As expected, by using N719 as dye, it was shown that bis(2,9-dimethyl-1,10-phenanthroline)copper ($[Cu(dmp)_2]^{2+}$), with a distorted tetragonal geometry, led to a higher cell efficiency (1.4%) than bis(1,10-phenanthroline)copper ($[Cu(phen)_2]^{2+}$) with a classical tetragonal geometry without any distortion (0.12%).[16] This beautifully underlines the crucial role of the geometry. More recently, using $[Cu(dmp)_2]^{2+/+}$ as electron mediator and a sterically hindered organic molecule (C218) as photosensitizer, a 7.0% efficiency was reached under solar illumination of 100 mW/cm^2; this efficiency was better than that obtained using the classic redox system I_3^-/I^- (6.5%).[17]

Also considering these interesting results, distorted tetrahedral copper(I) complexes with a rationally designed coordination sphere hold a great promise in their more positive redox potentials and smaller size with respect to hexacoordinated cobalt complexes, resulting in both potentially higher V_{oc} and higher diffusion limited photocurrents. On the other hand, one of their expected substantial disadvantages with respect to some Co(II) complexes based on bipyridine ligands, is a stronger absorption in the blue region of the visible spectrum, which may lead to light harvesting competition with the dye. Given these potential advantages and probable limitations, together with an easy tune ability of the redox potentials of Cu(I)/Cu(II) couple by an adequate choice of the ligands, it is interesting, in view of further developments, to systematically explore the electrochemical properties of a series of copper complexes, endowed with ligands having an increasing steric bulk around the copper central atom, investigating their response as DSSC redox mediators to different surface passivation treatments, cathode materials and to structurally different dyes. In particular, we investigated the effect of an increase in the π-delocalization of the phenanthroline ligand maintaining the methyl groups in internal 2 and 9 positions, comparing the behavior of $[Cu(2,9\text{-dimethyl-}1,10\text{-phenanthroline})_2]PF_6$ (**1**), with that of $[Cu(2,9\text{-dimethyl-}4,7\text{-diphenyl-}1,10\text{-phenanthroline})_2]PF_6$ complex[23] (**2**) (Figure1). Then, in order to understand the effect of a bulky substituent in position 2 of the phenanthroline ligands (i.e., very close to the copper central atom), we prepared the new complex $[Cu(2\text{-mesityl-}4,7\text{-dimethyl-}1,10\text{-phenanthroline})_2]PF_6$ (**3**). In this latter complex, there is a particular kiss lock because of the presence of one bulky substituent at the position 2 but only H at position 9 of the phenanthroline ligands. Because of the steric effect, the ligands are coordinated, keeping the mesityl groups on opposite sides of the copper center. This kiss lock could be a turning point to the development of novel efficient copper complex mediators for DSSCs, as suggested by our results.

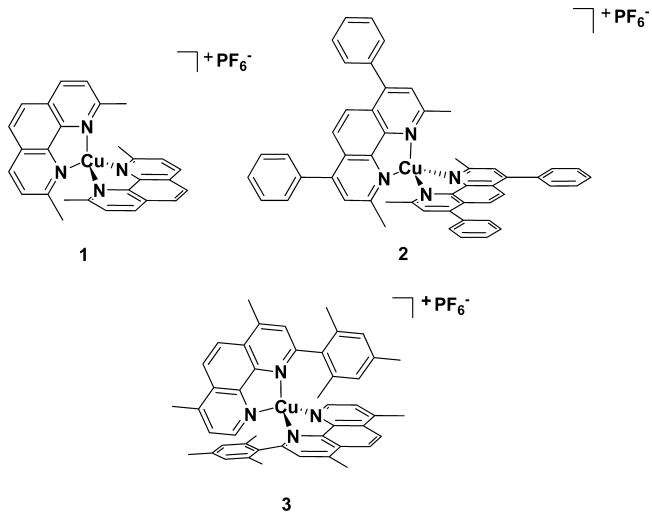

Figure 1. Structure of the Cu(I) complexes under investigation.

2. EXPERIMENTAL SECTION

2.1. Materials. Solvents for the synthesis were dried by standard procedures: *N*,*N*-dimethylformamide (DMF) was dried over activated molecular sieves and toluene was distilled over Na/benzophenone. All reagents were purchased from Sigma-Aldrich and were used without further purification. Reactions requiring anhydrous conditions were performed under argon or nitrogen. Thin layer chromatography (TLC) was carried out with precoated Merck F_{254} silica gel plates. Flash chromatography (FC) was carried out with Macherey-Nagel silica gel 60 (230−400 mesh). $Ru(LL')Cl_2$ (L = 4,4′dicarboxy-2,2′ bipyridine and L′ = 4,4′ dinonyl-2,2′ bipyiridine) was synthesized according to literature directions.[24]

2.2. Apparatus and Procedures. ^{1}H NMR and proton decoupled ^{13}C NMR spectra were recorded at 400 MHz (T = 300 K) on a Bruker Avance-400 instrument. Chemical shifts (δ) for ^{1}H spectra are expressed in ppm relative to internal Me_4Si as standard. Signals were abbreviated as s, singlet; d, doublet; dd, double doublet. Mass spectra were obtained with a FT-ICR Mass Spectrometer APEX II & Xmass software (Bruker Daltonics) 4.7 Magnet and Autospec Fission Spectrometer (FAB ionization).

Cyclic staircase voltammetry (CV) experiments were carried out in a small three-electrode cell (containing 3 cm^3 of the working solution) including: (i) as working electrode, a Teflon-embedded glassy carbon GC disk (Amel, surface 0.071 cm^2), (ii) a Pt sheet as counter-electrode and (iii) an aqueous saturated calomel electrode (SCE) as operating reference one inserted into a jacket filled with a solution of the same electrolyte used in the cell and ensuring contact with the working

Scheme 1. Preparation of New Ligand 2-Mesityl-4,7-dimethyl-1,10-phenanthroline (L3)[a]

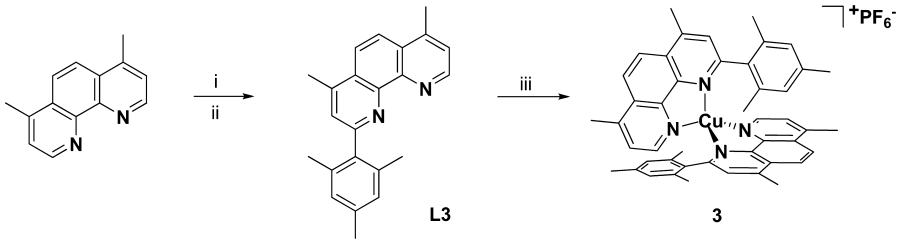

[a](i) mesityllithium, toluene, 0°C, r.t., 20 h; (ii) MnO_2 activated, toluene/DCM 5:3, r.t., 20 h; (iii) $[Cu(CH_3CN)_4]PF_6$, DMF, r.t. 20 min.

solution via a glass joint, in order to prevent water and chloride leakage in the working cell. The recorded potentials have been subsequently referred to the reference redox couple $Fc^+|Fc$ (ferriceniumlferrocene)[25] added as internal, or external, standard (ca. 1×10^{-3} M) at the end of each measures; in our conditions the half-wave potential of the $Fc^+|Fc$ couple was ca. 0.39 V vs SCE. The half-wave potentials, $E_{1/2}$, of all the reversible redox processes were calculated by CV pattern as the average value between the forward peak potential and the related backward one. Experiments were performed using an Autolab PGSTAT302N potentiostat/galvanostat (EcoChemie, The Netherlands) managed by a PC with GPES software. An instrumental compensation of the resistance (i.e., positive feedback) was carefully performed in order to minimize the ohmic drop between the working and reference electrode. The staircase CVs were performed with a 0.001 V step potential and at potential scan rate ranging between 0.02 and 2 V s^{-1}. The electrochemical analysis were carried out in dry acetonitrile (over molecular sieves, Sigma-Aldrich, ≥ 99.5%) containing ca. 1×10^{-3} M concentration of the sample with 0.1 M tetrabutylammonium hexafluorophosphate ($TBAPF_6$, Fluka, ≥ 99.0%) as supporting electrolyte. The working solution was well deareated by bubbling nitrogen before each measure starts and blowing it over the surface of the solution during the scans.

Transient absorption spectroscopy (TAS) was performed with a previously described apparatus,[26] by using the 532 nm harmonic of a nanosecond Nd:YAG laser (Continuum Surelite II). When performing TAS on transparent thin films, the excitation energy was reduced to ca. 5 mJ/cm^2/pulse by defocusing with a plano concave lens. A 532 nm notch filter prevented laser light from reaching the photomultipliter, whereas a 420 nm cut off filter, placed in front of the white light probe beam prevented direct TiO_2 excitation. From 10 to 30 laser shots, at a frequency of 0.2 Hz, were averaged to reach a good S/N ratio. Ru(III) recovery was monitored at 490 nm, corresponding to the minimum of the transient bleaching.

2.3. Synthesis of Copper Complexes. Copper complexes **1**−**3** were prepared and characterized following a procedure reported in the literature,[23,27] i.e., starting from Cu_2O, preparing the intermediate complex $[Cu(CH_3CN)_4]PF_6$, then adding two equivalents of the corresponding phenanthroline ligand. The new ligand 2-mesityl-4,7-dimethyl-1,10-phenanthroline (**L3**) was prepared by nucleophilic aromatic substitution of 4,7-dimethyl-1,10-phenanthroline with mesityllithium as a modification of a reported procedure (see Scheme 1).[28]

*Synthesis of 2-Mesityl-4,7-dimethyl-1,10-phenanthroline (**L3**).*

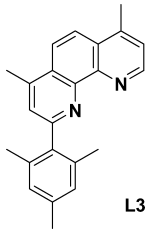

To a solution of bromomesitylene (5 mL, 17.4 mmol) in 54 mL of dry ether at −78 °C was slowly added *t*-BuLi (1.7 M in pentane, 20 mL, 34.8 mmol) under argon, and the solution was stirred for 10 min at −78 °C. The reaction mixture was warmed to room temperature gradually over 30 min, and the mixture was filtered through a glass filter under an argon pressure. The white solid was washed with 10 mL of dry ether under argon, dried under argon flow for 5 min and then dissolved in 8 mL of dry toluene. The solution of mesityllithium (2 mL, ca. 4 mmol) was added to a stirred suspension of 4,7-dimethyl-1,10-phenanthroline (300 mg, 1.4 mmol) in 10 mL of dry toluene cooled to 0 °C. The resulting deep-red solution was stirred overnight at room temperature.

Water (15 mL) was added. The layers were separated and the aqueous phase was extracted with dichloromethane (3 × 10 mL). The combined exctracts were stirred with an excess of activated manganese dioxide (2.5 g, 28.8 mmol) for 18h, by which time the intense yellow color of the solution has discarged. This mixture was dried over magnesium sulfate, filtered, and evaporated to give 400 mg of an amber oil. The recrystallization of crude product from a mixture of cyclohexane and acetone yielded 320 mg (70%) of the product as a white solid.

^{1}H NMR (400 MHz, $CDCl_3$): δ 9.08 (d, J(H−H) = 4.5 Hz, 1H), 8.11 (d, J(H−H)= 9.3 Hz, 1H), 8.06 (d, J(H−H)= 9.3 Hz, 1H), 7.44 (d, J(H−H) = 4.5 Hz, 1H), 7.41 (s, 1H), 6.93 (s, 2H), 2.84 (s, 3H), 2.83(s, 3H), 2.34 (s, 3H), 2.09 (s, 6H).

Elemental anal. Calcd (%) for $C_{23}H_{22}N_2$ (326.18): C, 84.63; H, 6.79; N, 8.58. Found: C, 84.61; H, 6.80; N, 8.56; MS (FAB^+) m/z: 326.

*Synthesis of [Cu(2-mesityl-4,7-dimethyl-1,10-phenanthroline)$_2$]-PF_6 (**3**).*

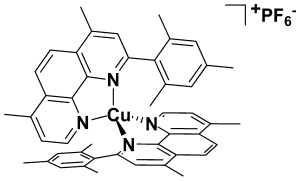

2-Mesityl-4,7-dimethyl-1,10-phenanthroline (50 mg, 0.15 mmol) was dissolved in dry DMF (70 mL) under a nitrogen atmosphere in a Schlenk vessel and then the Cu(I) precursor $[Cu(CH_3CN)_4][PF_6]$ (28 mg, 0.075 mmol) was added. The mixture, which instantaneously turned red, was stirred for 20 min at room temperature. After evaporation of the solvent, the desired complex was precipitated from MeOH/diethyl ether (v/v 1:10) to give a red complex that was dried under a vacuum (61 mg, 0.071 mmol, 95% yield).

^{1}H NMR (400 MHz, CD_2Cl_2): δ 8.78 (d, J(H−H) = 4.6 Hz, 1H), 8.25−8.18 (dd, J(H−H)= 16 Hz e 7 Hz, 2H), 7.61 (d, J(H−H) = 4.6 Hz, 1H), 7.36 (s, 1H), 6.21 (s, 1H), 5.82 (s, 1H), 2.93 (s, 3H), 2.88 (s, 3H), 1.97 (s, 3H), 1.71 (s, 3H), 1.06 (s, 3H). ^{13}C NMR (100 MHz, CD_2Cl_2): δ 158.2, 148.2, 146.6, 145.4, 143.9, 143.7, 137.2, 135.6, 134.8, 133.1, 128.3, 127.7, 127.0, 126.7, 126.2, 125.6, 122.4, 122.3, 20.7, 19.8, 19.1, 19.0, 18.9.

Elemental anal. Calcd for $C_{46}H_{44}CuF_6N_4P$ (860.25): C, 64.14; H, 5.15; Cu, 7.38; F, 13.23; N, 6.50; P, 3.60. Found: C, 64.09; H, 5.13; N, 6.52; MS (FAB^+) m/z: 715.

Synthesis of B5 Dye. 4.89 g of Ru(LL′)Cl_2 (L = 4,4′dicarboxy-2,2′ bipyridine and L′ = 4,4′ dinonyl-2,2′ bipyiridine) were dissolved in 450 mL of methanol; 18.9 g of KCN were added and the resulting mixture was refluxed under Ar for 3 h. The mixture was allowed to cool at room temperature and filtered. The solution was concentrated under rotary evaporation and the crude complex was precipitated by

cautious addition of aqueous HNO_3. (***Warning!*** *HCN evolves during this stage*). The orange solid was collected by suction filtration and washed with diluted HNO_3 (pH 3). The crude complex was purified by column chromatography (silica gel/methanol) and further reprecipitated by addition of aqueous HNO_3 affording B5 in 70% yield.

^{1}H NMR (400 MHz, CD_3OD) δ ppm: 9.8 d (1H), 9.4 d (1H), 9.0 s (1H), 8.95 s (1H), 8.5 s (1H), 8.4 s (1H), 8.15 d (1H), 7.8 s (2H), 7.6 d (1H), 7.4 d (1H), 7.15 d (1H), 2.9 t (2H), 2.7 t (2H), 1.8 t, broad (2H) 1.6 t, broad (2H), 1.5−1 m, broad (26H), 0.8 m (4H). ESI-MS: 805 u $(M\text{-}H^+)^-$; 851 u$[M+2Na]^-$

2.4. X-ray Structure of Complex 3. Crystals of complex **3** suitable for X-ray structure determination were obtained by crystallization from acetonitrile/diisopropylether (Figure 2, see Results and Discussion).

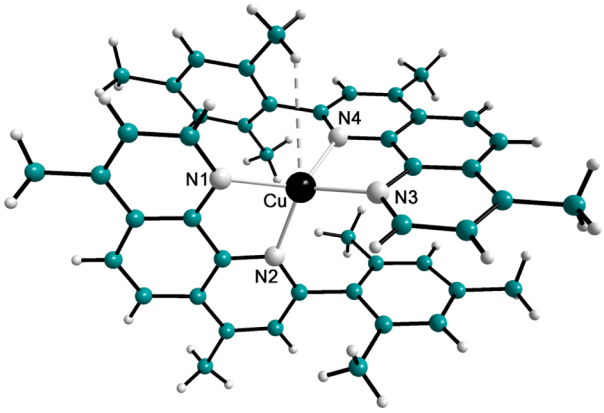

Figure 2. Perspective view of the $[Cu(2\text{-mesityl-}4,7\text{-dimethyl-}1,10\text{-phenanthroline})_2]^+$ cation. Selected interatomic distances (Å) and angles (deg) are Cu−N1 2.016(2), Cu−N2 2.084(2), Cu−N3 2.022(2), Cu−N4 2.066(2), N1−Cu−N2 81.54(6), N1−Cu−N3 141.82(7), N1−Cu−N4 122.24(6), N2−Cu−N3 114.07(6), N2−Cu−N4 120.05(6), N3−Cu−N4 81.43(6).

Crystal data. $C_{46}H_{44}CuF_6N_4P$, M = 861.36 g/mol, triclinic, a = 11.0766(7), b = 14.9354(10), c = 15.4651(10) Å, α= 103.10(1), β = 108.72(1), γ = 111.35(1) °, U = 2078.7(2) Å^3, T = 294(2) K, space group $P\bar{1}$ (No. 2), Z = 2, μ = (Mo−Kα) 0.629 mm^{-1}; 22144 reflections (12577 unique; R_{int} = 0.0240) were collected at room temperature in the range 1.80° < 2θ < 63.40°, employing a 0.16 × 0.04 × 0.02 mm^3 crystal mounted on a Bruker APEX II CCD diffractometer and using graphite-monochromatized Mo−Kα radiation (λ = 0.71073 Å). Data sets were corrected for Lorentz polarization effects and for absorption (T_{min} = 0.823) (SADABS).[29] The structure was solved by direct methods (SIR-97)[30] and was completed by iterative cycles of full-matrix least-squares refinement on F_o^2 and ΔF synthesis using the SHELXL-97[31] program (WinGX suite).[32] Hydrogen atoms, were located on the ΔF maps and allowed to ride on their carbon atoms. Final *R1* [*wR2*] values are 0.0508 [0.1498] on I > 2σ(I) [all data]. Crystallographic data for (**3**) (excluding structure factors) have been deposited with the Cambridge Crystallographic Data Centre as supplementary publication no. CCDC 1013866. These data can be obtained free of charge via www.ccdc.cam.ac.uk/conts/retrieving.html (or from CCDC, 12 Union Road, Cambridge CB2 1EZ, UK; fax: +44 1223 336033; e-mail: deposit@ccdc.cam.ac.uk).

2.5. DSSCs Fabrication. Conductive FTO glasses, ca. 8 Ω cm^2, was purchased from Pilkington (Merseyside, UK). Before use FTO glasses were cleaned with ethanol and sonicated for 10 min in an aqueous solution of Alconox (Sigma-Aldrich), then rinsed with abundant water and dried. Sandwich-type dye-sensitized solar cells were obtained coupling and pressing two FTO-based electrodes; a Parafilm sheet was used as insulating spaziator (ca. 100 μm thick) from which a mask was cutted in order to obtain, in the middle, a square hole that defined the active electrode area (0.25 cm^2) filled with ca. 10−20 μL of electrolyte solution; the sandwich was kept tightly together by two clips.

Electrolyte Solution Preparation. Three different samples were prepared containing 0.20, 0.15, and 0.10 M total concentration of copper complexes dissolving the desired amount of Cu(I) species in the suitable volume of ACN. Moreover three samples of different reduced/oxidized complex ratio were tested for each of the aformentioned concentrations, overall resulting in nine different electrolytes. The desired [Cu(II)]/([Cu(II)]+[Cu(I)]) ratio were obtained adding to each Cu(I) solution, containing $LiClO_4$ 0.1 M (Sigma-Aldrich), the appropriate volume of an oxidizing solution freshly prepared dissolving $NOBF_4$ (Sigma-Aldrich, 95%) in ACN, considering a 1:1 equiv ratio.

Photoanodes Preparation. A compact TiO_2 blocking underlayer was created prior to porous TiO_2 deposition: a freshly prepared precursor solution of titanium tetraisopropoxide, Ti(ip)$_4$, in 1-butanol was spin-coated onto cleaned FTO substrates (6 × 2.5 cm^2) at 1000 rpm for 9 s and at 2000 rpm for subsequent 25 s for three-times. The first time a 0.15 M Ti(ip)$_4$ solution was used, the second and third cycles a 0.3 M one. After the first two cycles the substrates were put in stove at 125 °C for ca. 5 min; after the third spin coating the resulting layer was baked at 500 °C for 15 min, resulting in a transparent compact 1.5 × 6 cm^2 TiO_2 film. The substrates were then cut into small 2.5 × 2 cm plates. Mesoporous TiO_2 films were obtained by casting over the compact TiO_2 underlayer a colloidal TiO_2 paste using the well-known adhesive tape casting method. The resulting film (2 × 0.5 cm^2) was sintered in an oven: from r.t. to 450 °C in 30 min, resting at 450 °C for 30 min; from 450 to 550 °C in 10 min resting at this temperature for 10 min. The final step involved the application of an aqueous 0.4 M $TiCl_4$ solution onto the mesoporous TiO_2 substrate for ca. 6 h, as it has been generally recognized that such treatment improves the photoelectrochemical properties of the DSSC.[33] Sensitization was carried out by immersion of the TiO_2 photoelectrodes in a ca. 1 × 10^{-5} M sensitizer solution in an appropriate solvent (or mixture). This procedure was carried out in the dark at room temperature for approximately 12 h. The photoanodes were rinsed with ethanol and immersed in 0.1% solution of (3-aminopropyl)triethoxysilane in toluene at 60 °C for 45 min; they were finally washed with toluene and acetonitrile.

Cathode Preparation. Cathode electrodes were poly(3,4-ethylenedioxythiophene)-modified FTO electrodes, PEDOT-FTO; they were obtained by electrooxidation of a 0.01 M solution of 3,4-ethylenedioxythiophene monomer in ACN with $LiClO_4$ 0.1 M as supporting electrolyte through a three-step potentiostatic anodic deposition. Experimental conditions: 0.2 V(SCE) for 5 s; 0.9 V(SCE) for 5 s; 1.6 V(SCE) for 30 s. The polymer-modified FTOs were then carefully rinsed many times with pure acetonitrile, dried and stored in air before cell assembling.

2.6. Electrochemical, Photoelectrochemical, and Spectroscopic Characterization. Estimation of the diffusion coefficients of the complexes was done through cyclic voltammetry on GC electrode in the aformentioned minicell of 3 cm^3 volume contaning ca. 0.001 M of sample. Two methods are employed,[34] averaging the corresponding results: (i) from the slope of the regression line of a $I_{p,ox}$ vs $\nu^{0.5}$ plot depicting the variation of the oxidation peak current, $I_{p,ox}$, as a function of the potential scan rate, ν; (ii) from the diffusion limited current, $I_{lim,ox}$, of the steady-state waves obtained through application of the semi-infinite convolution algorithm (a GPES facilities) to the experimental non-steady-state curves.

UV−visible absorption spectra were recorded using a Jasco V-530 spectrophotometer.

Polarization curves of symmetric cells and DSSCs were performed using staircase voltammetry adopting a two-electrode configuration at 0.005 or 0.02 V s^{-1} scan rate, using an Autolab PGSTAT101 potentiostat/galvanostat (EcoChemie, The Netherlands) managed by a PC with NOVA 1.10 software. Electrochemical impedance spectroscopy measurements were carried out on an Autolab PGSTAT302N potentiostat/galvanostat with a FRA module, using the following parameter set: 50 single wave frequencies, of 0.01 V amplitude, between 1 × 10^5 Hz and 1 × 10^{-2} Hz (logarithmic step).

J−*E* curves were recorded at 0.02 V s^{-1} under AM 1.5G 0.09 W/cm^2 illumination generated by an ABET sun simulator with the same electrochemical equipment described above.

Photoaction spectra of DSSCs were obtained with a custom-made apparatus comprising an air cooled Xe lamp (Luxtel, 175 W) coupled to an applied photophysics monochromator, adopting a 10 nm spectral bandwidth. Illuminated cell area was 0.25 cm^2. Photocurrents, sampled at 20 nm intervals, were recorded under short circuit conditions using an Agilent 34401A digital multimeter. Incident irradiances were measured by means of a Centronic OSD100−7Q calibrated silicon photodiode and the incident photon-to-electron conversion efficiency (IPCE) was calculated according to the formula

$$\text{IPCE\%} = 1240\frac{J}{\lambda W}$$

where J is the photocurrent density expressed in μA cm^{-2}, λ is the wavelength of incident monochromatic light, and W is the radiant power in W m^{-2}.

In all photoelectrochemical measurements under white light, the incident irradiance was 90 mW cm^{-2} under AM 1.5G conditions and the illumination was through the photoanode.

3. RESULTS AND DISCUSSION

3.1. Synthesis of Copper Complexes. Copper complexes **1**−**3** were prepared and characterized following a procedure reported in the literature,[23,24] i.e., starting from Cu_2O, preparing the intermediate complex $[Cu(CH_3CN)_4]PF_6$, then adding 2 equiv. of the corresponding phenanthroline ligand. The new ligand 2-mesityl-4,7-dimethyl-1,10-phenanthroline (**L3**) was prepared by nucleophilic aromatic substitution of 4,7-dimethyl-1,10-phenanthroline with mesityllithium as a modification of a reported procedure (see Experimental Section).[26]

3.2. Determination of the Crystal Structure of [Cu(2-mesityl-4,7-dimethyl-1,10-phenanthroline)$_2$]PF$_6$ (3). Crystals of complex **3** suitable for X-ray structure determination were obtained by crystallization from acetonitrile/diispropylether (Figure 2 and Figure S6 in the Supporting Information).

The $[Cu(2\text{-mesityl-4,7-dimethyl-1,10-phenanthroline})_2]^+$ cation displays the copper atom in a very distorted tetrahedral coordination, and interacts with its surrounding PF_6^- anions via weak C−H···F hydrogen bonds. The extent of distortion about copper is also related to the presence of a short intramolecular interaction of about 3.18 Å between the metal atom and a methyl substituent of one of the two ligands, resulting in an enlargement of the N1−Cu−N3 angle to 141.82(7)°.

3.3. Electrochemical and Spectrophotometric Study. The characterization of the electrochemical behavior of the copper-based reference complex **1**, its analogue **2**, and the new complex **3** (Figure 1) was dutiful in order to reveal their main redox properties essential for a rational assembly of the different components constituting a DSSC and for a critical interpretation of the photophysical and photoelectrochemical behavior of such devices.

The cyclovoltammetric study performed on glassy carbon electrode reveals two redox processes in the analyzed cathodic window and one in the anodic side (Figure 3), the former attributable to phenanthroline-based electron transfers that occur at less negative potential for complex **2** because of the presence of two phenyl rings that extend the π-conjugated system of the ligand.

Much more interesting for the purpose of this work is the metal-centered oxidation process being involved both in the dye regeneration step and in the mediator rereduction reaction at the counter electrode of a DSSC. The $Cu^{2+}|Cu^+$ oxidation peak is related to a monoelectronic, chemically reversible, and electrochemically quasi-reversible process characterized by comparable kinetics for all the three complexes (Table 1).

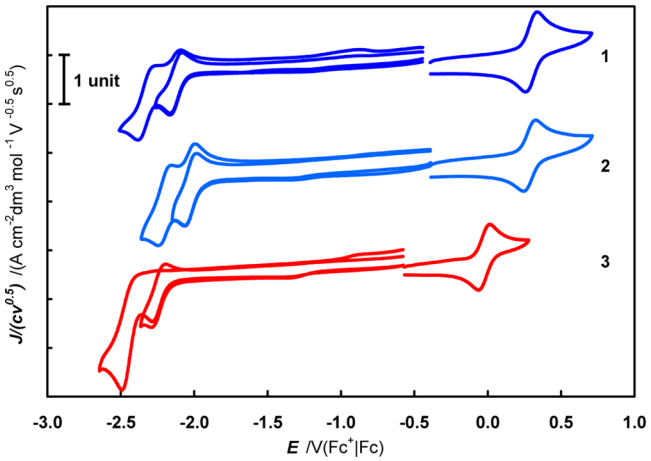

Figure 3. Synoptic normalized cyclovoltammograms of the three phenanthroline-based Cu(I) complexes (**1**−**3**) 0.001 M recorded on GC electrode (0.071 cm^2) in acetonitrile with 0.1 M $TBAPF_6$; scan rate 0.2 V s^{-1}.

Table 1. Electrochemical Properties of Cu(I) Mediators on Glassy Carbon Electrode in Acetonitrile with 0.1 M $TBAPF_6$

species	$E_{1/2,IRd}$ (V)[a]	$E_{1/2,Ox}$ (V)[a]	$E_{p,Ox}-E_{p/2,Ox}$ (V)[b]	$dE_{p,Ox}/d\log \nu$ (V)
1	−2.13	0.30	0.064	0.011
2	−2.03	0.29	0.067	0.013
3	−2.24	−0.02	0.060	0.013

[a]Potentials are referred to $Fc^+|Fc$ couple. [b]Obtained at ν = 0.2 V s^{-1}.

The oxidation half-wave potential, $E_{1/2,Ox}$, is significantly negative shifted (ca. 0.3 V) in the case of the kiss lock complex **3**, whereas it is essentially unchanged for the structurally analogue complexes **1** and **2**.

The net difference in the energetic of the $Cu^{2+}|Cu^+$ redox transition is rationalized by the different number of substituents in 2 and 9 positions of the phenanthroline that influences the flexibility of the metal-center geometry, which changes during the redox process.[22] In particular, a very recent paper[35] revealed that the increase in the number of substituents in 2 and 9 positions caused a progressive increase in the $Cu^{2+}|Cu^+$ oxidation potential (of an extent only slightly dependent by their actual steric hindrance); this was attributed to the progressive hampered transition from the preferred tetrahedral geometry of the Cu(I) reagent to the tetragonal one of the Cu(II) product. Moreover the direction of the peak potential shift was opposite to that induced by the electronic effects of the 2,9 substituents, confirming that the Cu(II) destabilization was mainly due to steric effects of the internal phenanthroline substituents.[35]

The cyclic voltammetries revealed that the diffusion coefficients of the complexes reflect their steric dimensions (see Table S1 in the Supporting Information), with the smaller complex **1** exhibiting the higher diffusion coefficient (1.0×10^{-5} cm^2 s^{-1}) that decreases for the complex **2** and **3** (6.5×10^{-6} and 6.6×10^{-6} cm^2 s^{-1}, respectively). Except for mediator **1** the diffusion coefficients are very similar to the ca. 6×10^{-6} cm^2 s^{-1} value observed for typical hexacoordinated Co(II) polypyridine complexes employed as mediators.[9]

In a DSSC, a fast Cu(I) regeneration at the counter electrode is mandatory to minimize the cathodic overpotential; as a consequence, the choice of an appropriate cathodic substrate is fundamental to maximize the V_{oc}. Polarization curves (see Figure S1 in the Supporting Information) recorded in symmetric cells

(i.e., anode and cathode electrodes of the same material) with bare FTO and PEDOT-modified FTO electrode show that the PEDOT film constitutes a better cathodic substrate offering a lower overpotential to the heterogeneous electron transfer. The exchange current density J_0 is equal to 1.7×10^{-4} A cm^{-2} for FTO and 2.0×10^{-3} A cm^{-2} for PEDOT-modified electrode; the transfer coefficient is the same for both substrates, *c*a. 0.5. The limiting current in the presence of PEDOT counter electrodes separated by a sealant ca. 100 μm thick is of the order of 10 mA cm^{-2}, setting the upper limit to the hypothetical short circuit photocurrent delivered by an equivalent DSSC operating under pure diffusional control.

An other importante feature of a suitable redox shuttles is that they shuold compete as less as possible with the sensitizer for visible light harvesting. The spectroscopic characterization of the complexes **1**−**3** in ACN (Figure 4) showed in the visible

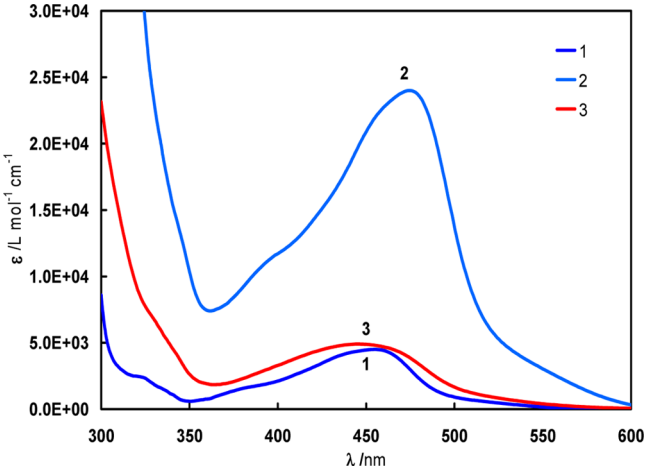

Figure 4. Synopsis of visible spectra of the three Cu(I)-based redox mediators **1**−**3** in ACN.

region a broad absorption band, ranging up to 445−475 nm, related to a metal-to-ligand charge transfer transition, MLCT.[36] According to the more extended π-conjugated system guaranteed by the two phenyl rings, complex **2** exhibited the lowest absorption wavelength (i.e., 475 nm) because of the decreased HOMO−LUMO gap and the highest molar absorptivity (i.e., 2.4×10^4 L mol^{-1} cm^{-1}) compared to ca. 5×10^3 L mol^{-1} cm^{-1} for complex **1** and **3**. So all the complexes showed limiteted molar absorptivity; in particular, for samples **1** and **3** they are about one order of magnitude lower than those of typical dyes employed in DSSCs.

3.4. Dye-Sensitized Solar Cells. *Photoanode Silanization.* Tests, performed on photoanodes constituted by mesoporous TiO_2 deposited on the FTO surface, clearly revealed an undesired efficient electron capture by copper mediators (i.e., recombination process) that brought to a total absence of photocurrent. The parasitic reaction was only partially diminished through the preparation of two-layer photoanodes (a mesoporous TiO_2 layer over an underlying compact one) suggesting that, probably, the recombination largely occurred on the exposed FTO surface in agreement with the modest overpotential to the electron capture offered by this substrate (see Figure S1 in the Supporting Informaiton). An additional silanization step of the bilayer sensitized photoanodes brought to an extraordinary increase (ca. 3×) of the cell efficiency (Figure 5). The silanized photoanodes were used in all subsequent experiments.

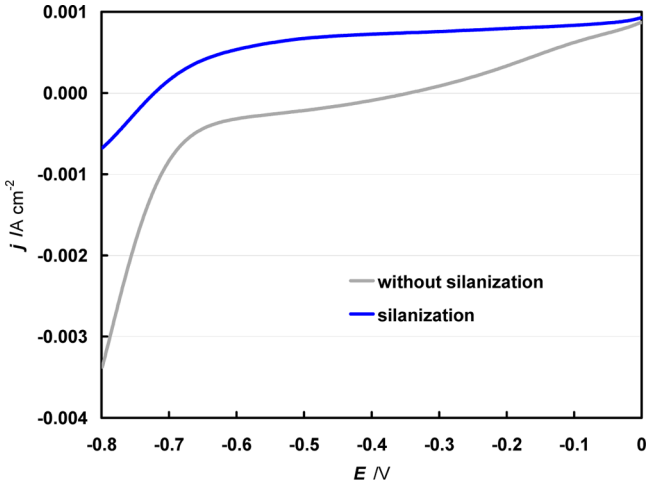

Figure 5. Normalized *J*−*E* characteristics of sandwich-type DSSCs employing bilayer TiO_2 photoanode without silanization (gray line) and after silanization (blue line) sensitized with [Ru(dcbpy)$_2$(dnbpy)](PF6)$_2$ dye, under 90 mW cm^{-2} AM 1.5G illumination. Electrolyte composition: 0.1 M solution of mediator **1** (5% of Cu(II) form) in acetonitrile plus 0.1 M $LiClO_4$. Scan rate: 0.005 V s^{-1}.

DSSCs were prepared with the following dye sensitizers: Z907,[24] MK2,[37] B5, and [Ru(dcbpy)$_2$(dnbpy)](PF$_6$)$_2$ (Figure 6), where dcbpy and dnbpy are 4,4′-dicarboxy-bipyridine and 4,4′-dinonyl-bipyridine, respectively.[38]

Cell performances showed a marked dependence on the molecular features of the dyes. With some dyes the *J*−*E* curve of the DSSC under illumination showed only a cathodic current flow (MK2 > Z907 > B5) with a pattern very similar to that obtained in the dark (see Figure S2 in the Supporting Information), meaning that charge recombination processes involving conduction band electrons were obscuring photocurrent generation. This phenomenon could be related to the presence of coordinating groups on the dye molecule (especially if sulfur atom is present), which could, at least in principle, interact with the copper complexes characterized by a well-known polyhedric geometry (from 4 to 6 coordination sites).[22] This would be the case of the thiophene-based sensitizer, MK2, and of two bis-bipyridine Ru(II) dyes, Z907 and B5, bearing thiocyanate and cyano ancillary groups, respectively, as a matter of fact the only complex showing some photocurrent generation was the tris-chelated Ru(II) dye. However, the detailed nature of the phenomenon was not studied in more detail.

Starting from this screening all the subsequent experiments were performed on DSSCs employing the [Ru(dcbpy)$_2$(dnbpy)](PF$_6$)$_2$ complex as sensitizer.

3.5. Copper Mediator Performances. The polarization curves and the impedance spectra of the DSSCs under illumination, together with the corresponding dark currents, were collected and analyzed in order to rationalize the electrochemical behavior of the three Cu(I) complexes (Figure 7, and Figures S3 and S4 in the Supporting Information). As expected, complexes **1** and **2** show essentially the same cell parameters (Table 2, Figure 7) coherently with quite the same structure and the similar electrochemical behavior (i.e., half-wave potential and electrochemical quasi-reversibility). Of relevance is the ca. 0.72 V open circuit photovoltage generated by these easily synthesizable mediators that can be attributed to their extremely positive half-wave potential value. At the same time, their positive potential, coupled to a substantial reorganization

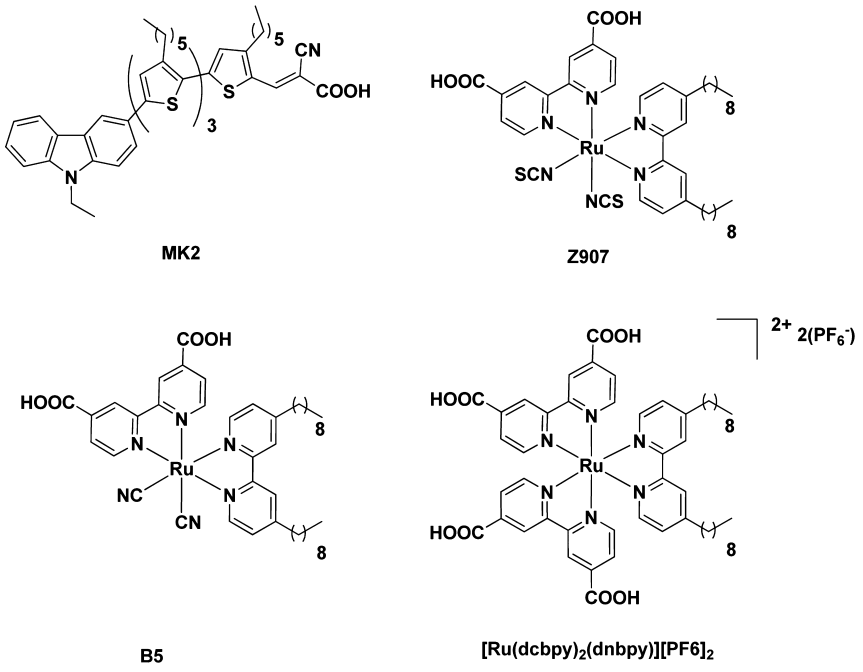

Figure 6. Structure of the sensitizers used for DSSCs.

energy, may also result in a slow dye regeneration rate, leading to modest photocurrents, which determine a low power conversion efficiency (ca. 30% of that observed with the I_3^-/I^- electrolyte).

Interesting are the performances recorded with the novel asymmetric phenanthroline-based complex **3**: except for the expected diminished V_{oc}, which however nearly matches the value of I_3^-/I^-, all other cell parameters undergo a net improvement; in particular, the improved J_{sc} results in the doubling of η with respect to complexes **1** and **2**, reaching ca. 50% of the power conversion obtained with the benchmark iodide-based electrolyte (Table 2).

Considering the promising performances of the Cu(I) electron transfer mediator **3**, a deeper study on the influence of the total concentration of the mediator and of the Cu(II)/Cu(I) ratio was carried out (see Table S2 and Figure S7 in the Supporting Information). As expected, the increase of the total concentration of the mediator leads to an increase of the short-circuit currents, but unfortunately this improvement is accompanied by a net decrease in the photovoltage, making the cell efficiency essentially independent of the mediator concentration. Moreover, in all cases, electron mediator **3** showed slightly worse photoaction behavior than the benchmark electrolyte, coherently with its stronger competition to visible-light harvesting with the dye in regards to iodine-based solution.

Electrochemical impedance spectroscopy (Figures 7 and Figure S4 in the Supporting Information) is useful to rationalize the significantly different performances of complex **3** with respect to the structurally related **1** and **2**. No significant resistance for the charge transfer at the PEDOT counter electrode was detected in all the systems under examination. The mass-transport resistance, evident at lower frequencies, does not seem to be particularly relevant for the total cell impedance.

On the contrary the electron lifetime in the titanium dioxide, $\tau_{e\text{-}(TiO2)}$, is more than doubled, going from ca. 2 ms for the 2,9-dimethyl-substituted phenanthroline-based copper mediators (**1**, **2**) to ca. 5 ms of the 2-mesityl-substituted phenanthroline-based copper complex **3** (Figure 7), suggesting that with the latter species the parasitic charge recombination process is, somehow, drastically reduced, allowing a more efficient generation of photocurrent. It is not straightforward to determine whether the increased electron lifetime observed with **3** arises from a superior dye regeneration (and hence from a reduced dye^+/e^- recapture) or by a slower recombination kinetics involving Cu(II) centers in the electrolyte. The inspection of the dark currents indicates that, at low forward potential (<− 400 mV) mediator **3**, is characterized by a lower recombination current with respect to the other two copper-based species (blue lines in Figure S3 in the Supporting Information). However, at potentials more negative than − 500 mV Cu(II) reduction in **3** proceeds faster than in **1** and **2**, consistent with the lower photovoltage observed with such complex. In general, however, the dark current observed with **3** is slightly lower than that observed with the I_3^-/I^- couple. Transient absorption spectroscopy, carried out at excitation energies of ca. 5 mJ/(cm^2 pulse), higher than those experienced under solar illumination, did not reveal large differences in the dye regeneration rate, as both **3** and **1** complexes showed similarly slow electron transfer kinetics with respect to 0.1 M lithium iodide, where the facile electron donation by I^- results in a Ru(III) half-life of ca. 15 ns. In the presence of both Cu(I) species (Figure 8), the faster initial part of the decay is slightly accelerated in the order **3** >**1**, whereas the slowest part of the decay follows a kinetic that is almost superimposable to that observed in the presence of the inert 0.1 M $LiClO_4$ electrolyte (Ru(III) half-life of 96 ns), where the Ru(II) recovery occurs solely by recapture of the photoinjected electrons by Ru(III). It is interesting that both copper mediators under investigation (**1** and **3**) exhibit similarly slow electron transfer kinetics despite the significant difference in their $E_{1/2}$, which should result in a larger driving force for Ru(III) reduction by complex **3**. This implies that probably the increased ΔG° is compensated by a larger reorganization energy change associated with the $Cu^{2+}|Cu^+$ transition in **3**, or that the electronic coupling rather than the nuclear factor is playing the major role in determining the electron transfer rate from Cu(I) to Ru(III).

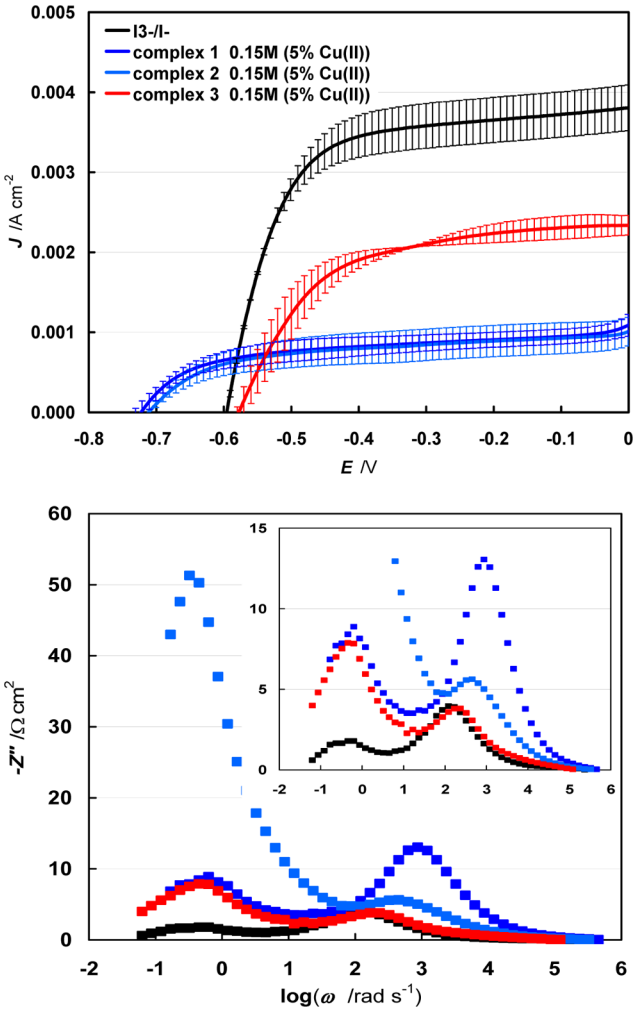

Figure 7. Top: normalized J–E curves of DSSCs (active area 0.25 cm^2) employing the three Cu(I) mediator complexes recorded under 90 mW cm^{-2} AM 1.5G illumination. For sake of comparison, the reference redox couple I_3^-/I^- in the same condition (black line) is also reported. Bottom: normalized imaginary impedance plots of the same cells; inset: magnification of the high-frequency peaks.

3.6. Electron Comediator Effects. Considering that sluggish regeneration of the oxidized dye by Cu(I) represents the main limitation to cell efficiency, we explored the effect of the addition of an electron comediator to the electrolytic solution, as it was done in previous studies, where the presence of small amounts (ca. 10%) of phenothiazine or iron complexes in the electrolyte solution containing Co(II) tris-bipyridyl was observed to lead to a remarkable increase of photocurrent intensity.[9,39−42] Obviously the half-wave potential of the comediator has to be intermediate between that of the dye and of the mediator, in order to ensure the exoergonicity of both the heterogeneous and homogeneous electron transfer with the adsorbed dye and the main mediator, respectively.

For our scope, two bipyridine-based iron complexes have been chosen: tris(4,4′-dimethoxy-2,2′-bipyridine)Fe(II), $[Fe(dmo\text{-}bpy)_3]^{2+}$,[42] and tris(4,4′-ditertbutyl-2,2′-bipyridine)Fe(II), $[Fe(dtb\text{-}bpy)_3]^{2+}$,[39] bis-hexafluorophosphate, having $E_{1/2}$ = 0.36 V vs $Fc^-|Fc$ and $E_{1/2}$ = 0.44 V vs $Fc^-|Fc$, respectively.

The addition of the comediators brings in all cases a decrease in the V_{oc} (more evident for **3** than **1**) and the fill factor, FF, but an increase in the photocurrent (Table 2).

Table 2. Main Cell Parameters Employing One-Component Electrolytes (copper mediator) and Bicomponent Ones (copper mediator with an iron co-mediator) with $[Ru(dcbpy)_2(dnbpy)](PF_6)_2$ Dye[a]

electrolyte[b]	V_{oc} (V)	J_{sc} (mA cm^{-2})	FF	η (%)	$\tau_{e\text{-}(TiO2)}$ (ms)[c]
0.15 M (**1**)	0.73	1.1	0.50	0.4	1
0.10 M (**1**)	0.72	0.9	0.53	0.4	
0.15 M (**2**)	0.71	1.1	0.49	0.4	2
0.15 M (**3**)	0.58	2.4	0.58	0.9	5
0.10 M (**3**)	0.60	2.0	0.64	0.9	6
0.10 M (**3**) + 0.01 M $[Fe(dmo\text{-}bpy)_3]^{2+}$	0.55	2.7	0.49	0.8	11
0.10 M (**3**) + 0.01 M $[Fe(dtb\text{-}bpy)_3]^{2+}$	0.51	4.0	0.51	1.2	10
0.10 M (**3**) + 0.01 M $[Fe(dtb\text{-}bpy)_3]^{2+}$ + 0.1 M t-But-py	0.62	1.7	0.69	0.8	6
0.10 M (**1**) + 0.01 M $[Fe(dtb\text{-}bpy)_3]^{2+}$	0.67	1.3	0.50	0.5	1
I_3^-/I^-	0.60	3.8	0.66	1.7	8

[a]Irradiation of 90 mW cm^{-2} simulated AM 1.5G sunlight. All data are averaged from two independent DSSCs under the same experimental conditions. [b]The samples are dissolved in ACN with $LiClO_4$ 0.1 M; in all cases, [Cu(II)]/([Cu(II)]+[Cu(I)]) = 0.05. [c]From EIS measurements.

In particular, in the case of complex **3**, even if the improvement is modest with the $[Fe(dmo\text{-}bpy)_3]^{2+}$, the butyl derivative raises the photocurrent at a value slightly higher than that obtained by the benchmark iodine-based electrolyte (Figure 9, Table 2 and Figure S5 in the Supporting Information) and the cell efficiency at comparable value.

The different performances of the "binary" electrolyte solutions were also studied recording photoaction spectra. The choice of the sensitizer ($[Ru(dcbpy)_2(dnbpy)]^{2+}$) and of formally identical photoanode substrates having identical treatments sets the injection quantum yield Φ_{inj} and the light harvesting efficiency (LHE), therefore the different photon-to-current conversion efficiencies, IPCEs, can only be explained by different electron collection efficiencies (η). Collection efficiency is limited by recombination involving both the oxidized dye (Ru(III)) and the oxidized electron mediator (Cu(II)). Given that the Ru(III) regeneration by Cu(I) is slow, the addition of a kinetically faster couple having a small reorganization energy, like the Fe(II)/Fe(III) complexes, allowing for a faster Ru(III) reduction, should result in an increased electron collection efficiency, leading to an improved photon-to-electron conversion. Transient absorption spectroscopy (Figure 9) allowed to verify that, with respect to the simpler case of complex **3** as unique component of electrolyte, the addition of a relatively small percentage (10% mol/mol) of Fe(II)-based mediator brings a slight acceleration of the Ru(II) recovery, particularly in the fast part of the decay, resulting in a half-life of 79 ns in the case of tertbutyl-bipyridine derivative and of 43 ns in the case of $[Fe(dmo\text{-}bpy)_3]^{2+}$. The superior regeneration capabilities of $[Fe(dmo\text{-}bpy)_3]^{2+}$/**3** mixture is motivated by the superior driving force of the former with respect to $[Fe(dtb\text{-}bpy)_3]^{2+}$ but also, possibly, by the stronger electronic coupling resulting from the lack of bulky *tert*-butyl substituents.

The partial suppression of the Ru(III)/e^- recapture, following addition of the comediator results indeed in nearly doubled electron lifetimes (10 and 11 ms in the presence of Fe(II) comediators) determined by EIS experiments at V_{oc} (Table 2).

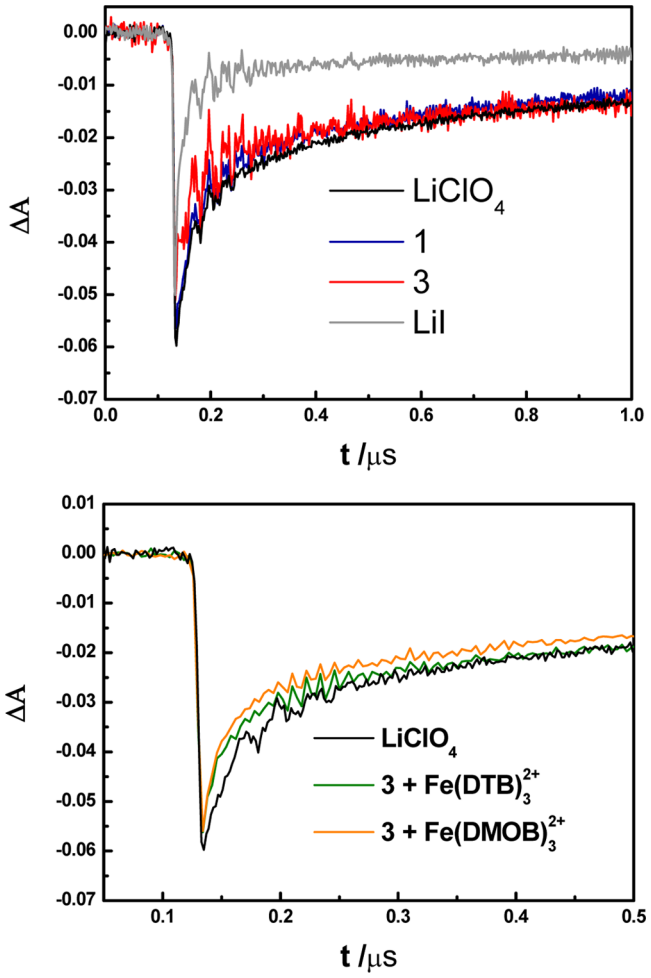

Figure 8. Top: 490 nm recovery of $[Ru(dcbpy)_2(dnbpy)](PF_6)_2$ dye loaded on mesoporous TiO_2 electrode in the presence of inert electrolyte acetonitrile with 0.1 M $LiClO_4$ (black line); 0.1 M Cu(I) + 0.1 M Li^+ (complex **3**, red line, and complex **1**, blue one); 0.1 M LiI (gray line). Bottom: Ru(II) recovery in the presence of inert electrolyte (black line); 0.1 M complex **3** + 0.1 M Li^+ + 0.01 M $[Fe(dtb\text{-}bpy)_3]^{2+}$ (green); 0.1 M complex **3** + 0.1 M Li^+ + 0.01 M $[Fe(dmo\text{-}bpy)_3]^{2+}$ (orange). Laser excitation: λ_{exc} = 532 nm, 5 mJ/cm^2/pulse.

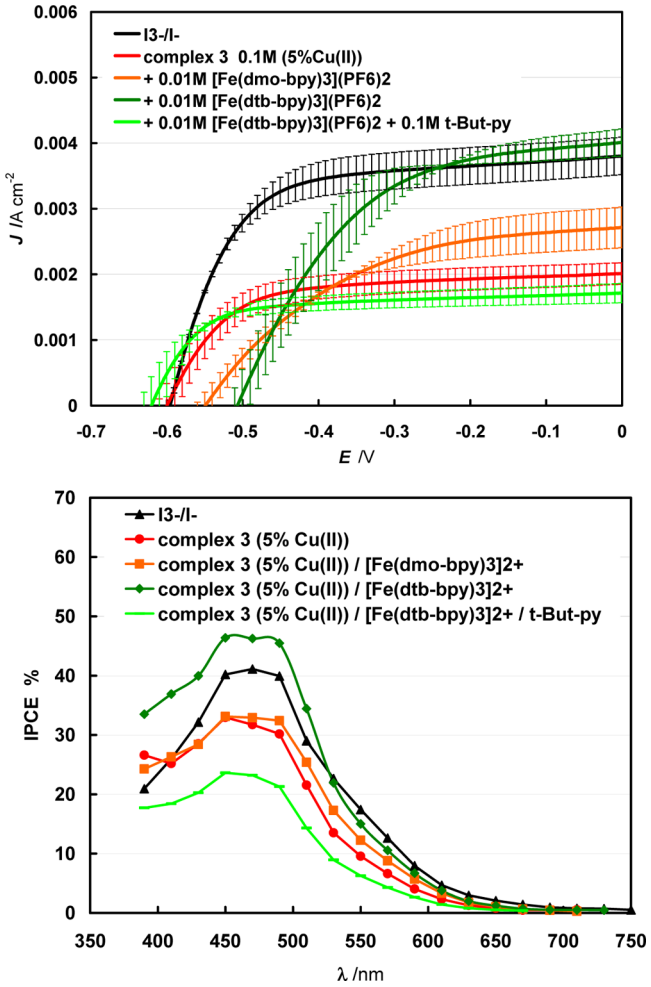

Figure 9. Top: normalized *J*–*E* characteristics of DSSCs (active area 0.025 cm^2) employing copper complex **3** as such and in 10:1 molar ratio mixture with Fe(II)-based comediators; 90 mW cm^{-2} AM 1.5G illumination. Composition: 0.1 M copper-based mediator (with 5% of Cu(II) form) and 0.01 M comediator $[Fe(dmo\text{-}bpy)_3](PF_6)_2$ (orange) or $[Fe(dtb\text{-}bpy)_3](PF_6)_2$ (dark green). Light green curve represents the effect of an addition of 0.1 M t-But-py to $[Fe(dtb\text{-}bpy)_3]^{2+}$/**3** mixture. Black line reported for sake of comparison is the same as in Figure 7. Bottom: corresponding photoaction spectra.

The highest IPCE (ca. 50% at 470 nm) was recorded with the $[Fe(dtb\text{-}bpy)_3]^{2+}$/**3** mixture (Figure 9) which has an inferior regeneration kinetics with respect to $[Fe(dmo\text{-}bpy)_3]^{2+}$/**3**, indicating that the secondary electron transfer step involving the reduction of Fe(III) by Cu(I) is also critical in determining the success of the binary electrolyte, as pointed out in previous works.[44−47] The $[Fe(dtb\text{-}bpy)_3]^{3+/2+}$ couple possesses a larger driving force for the oxidation of Cu(I) (ca. 0.44 eV), leading to a faster regeneration of Fe(II), and bulky *tert*-butyl chains, which may contribute to decouple Fe(III) from the TiO_2 surface, both characteristics being instrumental in decreasing the efficiency of electron recapture involving Fe(III) and electrons trapped in the TiO_2.

As a final test the effect of *tert*-butylpyridine (t-But-py), usually employed as an additive to improve the V_{oc} of the cells was evaluated.[44−47] The addition of t-But-py 0.1 M to the most performing binary mixture $[Fe(dtb\text{-}bpy)_3]^{2+}$/**3** caused a loss in term of cell efficiency due to a deep decrease of the photogenerated current (Figure 9, Table 2) not compensated by the increase in open circuit potential. This adverse effect is ostensibly related to a decreased charge injection efficiency of the dye, caused by the upward shift of the TiO_2 Fermi level and possibly by the coordination of t-But-py to the tetragonally distorted Cu(II), causing a modification of the thermodynamic and kinetic properties of the redox mediator.

4. CONCLUSIONS

In the context of the development of new performing mediator redox couples that could efficiently substitute the more common I_3^-/I^- one, we have proposed two phenanthroline-based Cu(I) complexes obtainable in high yields through convenient and easily accessible synthetic pathway. The new complex $[Cu(2\text{-mesityl-}4,7\text{-dimethyl-}1,10\text{-phenanthroline})_2]PF_6$ (**3**) is of particular interest because the presence of the bulky mesityl groups on the phenanthrolines protect as a kiss lock the copper center, leading to slightly superior dye regeneration kinetics and longer electron lifetimes with respect to simpler 2,9-dimethyl-phenanthroline based Cu(I) complexes, as a result of a dark current lower than that observed with the I_3^-/I^- couple. These

results, however, could be achieved only after a careful choice of the dye and suitable TiO_2 passivation strategies, based on the coadsorption of alkyl-siloxanes. In combination with [Ru(4,4′-dicarboxy-2,2′-bipyridine)$_2$(4,4′-dinonyl-2,2′-bipyridine)]-$(PF_6)_2$ dye, the new complex **3** revealed interesting relative improvements with respect to the best performing copper mediator reported in the literature, $[Cu(2,9\text{-dimethyl-}1,10\text{-phenanthroline})_2]^+$ (**1**), doubling both the photocurrent and the overall cell conversion efficiency. The study of Ru(II) recovery kinetics demonstrated that one of the main limitation of this family of copper complexes is related to the slow dye regeneration, which could be improved by addition of a 10% molar amount of a kinetically fast poly pyridine Fe(II) comediator, which resulted in a considerable increase of photocurrent. The exploitation of a dual-component electrolyte constituted by **3** and $[Fe(4,4'\text{-ditertbutyl-}2,2'\text{-bipyridine})_3][PF_6]_2$ allowed to increase the performance of the cell reaching J_{sc} values (4.0 mA cm^{-2}) comparable to that recorded with the I_3^-/I^- redox couple (3.8 mA cm^{-2}).

On account of these comparative cell performances, these new Cu(I) complexes show promise as outer-sphere electron transfer mediators, likewise some of the best-known cobalt complexes. Given the strong dependence of the mediator performance on the nature of the dye, as also shown by recent works,[12,13] studies will now be directed in developing optimized dyes for these new redox mediators.

■ ASSOCIATED CONTENT

Supporting Information

Normalized polarization curves of symmetric cells, normalized *J*–*E* curves, normalized dark currents, normalized Nyquist diagrams, cell parameters and photoaction spectra for DSSC employing mediator **3** at different total concentrations and Cu(II)/Cu(I) ratio, additional X-ray structure of complex **3**, and detailed diffusion coefficient data. This material is available free of charge via the Internet at http://pubs.acs.org.

■ AUTHOR INFORMATION

Corresponding Authors

*E-mail: alessia.colombo@unimi.it.
*E-mail: mirko.magni@unimi.it.
*E-mail: cte@unife.it.

Notes

The authors declare no competing financial interest.

■ ACKNOWLEDGMENTS

Dr. Rita Boaretto (University of Ferrara) is acknowledged for the synthesis of the B5 dye. We are thankful to Ms. Laura Casarin (University of Ferrara) for the kind technical assistance. This work was supported by MIUR (PRIN 2010, 20104XET32).

■ DEDICATION

Dedicated to Prof. Renato Ugo for his 76th birthday

■ REFERENCES

(1) O'Regan, B.; Graetzel, M. A Low-cost, High-efficiency Solar Cell Based on Dye-sensitized Colloidal TiO_2 Films. *Nature* **1991**, *353*, 737–740.
(2) Graetzel, M. Photoelectrochemical Cells. *Nature* **2001**, *414*, 338–344.
(3) Bredas, J.-L.; Durrant, J. R. Organic Photovoltaics. *Acc. Chem. Res.* **2009**, *42*, 1689–1690.
(4) Nozik, A. J.; Miller, J. Introduction to Solar Photon Conversion. *Chem. Rev.* **2010**, *110*, 6443–6445.
(5) Wong, W. Y.; Ho, C. L. Organometallic Photovoltaics: A New and Versatile Approach for Harvesting Solar Energy Using Conjugated Polymetallaynes. *Acc. Chem. Res.* **2010**, *43*, 1246–1256.
(6) Hagfeldt, A.; Boschloo, G.; Sun, L.; Kloo, L.; Pettersson, H. Dye-sensitized Solar Cells. *Chem. Rev.* **2010**, *110*, 6595–6663.
(7) Snaith, H. J. Estimating the Maximum Attainable Efficiency in Dye-Sensitized Solar Cells. *Adv. Funct. Mater.* **2010**, *20*, 13–19.
(8) Nazeeruddin, M. K.; Baranoff, E.; Graetzel, M. Dye-sensitized Solar Cells: A Brief Overview. *Sol. Energy* **2011**, *85*, 1172–1178.
(9) Bignozzi, C. A.; Argazzi, R.; Boaretto, R.; Busatto, E.; Carli, S.; Ronconi, F.; Caramori, S. The Role of Transition Metal Complexes in Dye Sensitized Solar Devices. *Coord. Chem. Rev.* **2013**, *257*, 1472–1492.
(10) Yella, A.; Lee, H.-W.; Tsao, H. N.; Yi, C.; Chandiran, A. K.; Nazeeruddin, M. K.; Diau, E. W.-G.; Yeh, C.-Y.; Zakeeruddin, S. M.; Graetzel, M. Porphyrin-sensitized Solar Cells with Cobalt (II/III)-based Redox Electrolyte Exceed 12% Efficiency. *Science* **2011**, *334*, 629–634.
(11) Colombo, A.; Dragonetti, C.; Roberto, D.; Valore, A.; Biagini, P.; Melchiorre, F. A Simple Copper(I) Complex and Its Application in Efficient Dye Sensitized Solar Cells. *Inorg. Chim. Acta* **2013**, *407*, 204–209.
(12) Bozic-Weber, B.; Chaurin, V.; Constable, E. C.; Housecroft, C. E.; Meuwly, M.; Neuburger, M.; Rudd, J. A.; Schönhofer, E.; Siegfried, L. Exploring Copper(I)-Based Dye-Sensitized Solar Cells: a Complementary Experimental and TD-DFT Investigation. *Dalton Trans.* **2012**, *41*, 14157–14169.
(13) Bozic-Weber, B.; Brauchli, S. Y.; Constable, E. C.; Furer, S. O.; Housecroft, C. E.; Wright, I. A. Hole-Transport Functionalized Copper(I) Dye Sensitized Solar Cells. *Phys. Chem. Chem. Phys.* **2013**, *15*, 4500–4504.
(14) Hewat, T. E.; Yellowlees, L. J.; Robertson, N. Neutral Copper(I) Dipyrrin Complexes and Their Use as Sensitizers in Dye-Sensitized Solar Cells. *Dalton Trans.* **2014**, *43*, 4127–4136.
(15) Bozic-Weber, B.; Brauchli, S. Y.; Constable, E. C.; Fürer, S. O.; Housecroft, C. E.; Malzner, F. J.; Wright, I. A.; Zampese, J. A Improving the Photoresponse of Copper(I) Dyes in Dye-Sensitized Solar Cells by Tuning Ancillary and Anchoring Ligand Modules. *Dalton Trans.* **2013**, *42*, 12293–12308.
(16) Hattori, S.; Wada, Y.; Yanagida, S.; Fukuzumi, S. Blue Copper Model Complexes with Distorted Tetragonal Geometry Acting as Effective Electron-transfer Mediators in Dye-Sensitized Solar Cells. *J. Am. Chem. Soc.* **2005**, *127*, 9648–9654.
(17) Bai, Y.; Yu, Q.; Cai, N.; Wang, Y.; Zhang, M.; Wang, P. High-efficiency Organic Dye-Sensitized Mesoscopic Solar Cells with a Copper Redox Shuttle. *Chem. Commun.* **2011**, *47*, 4376–4378.
(18) Gray, H. B.; Solomon, E. I. *Copper Proteins*; Spiro, T. G., Ed.; Wiley: New York, 1981; pp 1–39;.
(19) Sykes, A. G. Active-Site Properties of the Blue Copper Proteins. *Adv. Inorg. Chem.* **1991**, *36*, 377–408.
(20) Adman, E. T. Copper Protein Structures. *Adv. Protein Chem.* **1991**, *42*, 145–197.
(21) Gross, E. L. Plastocyanin: Structure and Function. *Photosynth. Res.* **1993**, *37*, 103–116.
(22) Rorabacher, D. B. Electron Transfer by Copper Centers. *Chem. Rev.* **2004**, *104*, 651–697.
(23) Ruthkosky, M.; Castellano, F. N.; Meyer, G. J. Photodriven Electron and Energy Transfer from Copper Phenanthroline Excited States. *Inorg. Chem.* **1996**, *35*, 6406–6412.
(24) Wang, P.; Zakeeruddin, S. M.; Moser, J. E.; Nazeeruddin, M. K.; Sekiguchi, T.; Graetzel, M. A Stable Quasi-Solid-State Dye-Sensitized Solar Cell with an Amphiphilic Ruthenium Sensitizer and Polymer Gel Electrolyte. *Nat. Mater.* **2003**, *2*, 402–407.
(25) Gritzner, G.; Kuta, J. Recommendations on Reporting Electrode Potentials in Nonaqueous Solvents. *Pure Appl. Chem.* **1984**, *56*, 461–466.

(26) Mba, M.; D'Acunzo, M.; Salice, P.; Carofiglio, T.; Maggini, M.; Caramori, S.; Campana, A.; Aliprandi, A.; Argazzi, R.; Carli, S.; Bignozzi, C. A. Sensitization of Nanocrystalline TiO_2 with Multi-branched Organic Dyes and Co(III)/(II) Mediators: Strategies to Improve Charge Collection Efficiency. *J. Phys. Chem. C* **2013**, *117*, 19885−19896.
(27) Kubas, G. J. Tetrakis(acetonitrile)copper(I)-hexafiuorophosphate. *Inorg. Synth.* **1979**, *19*, 90−92.
(28) Jakobsen, S.; Tilset, M. A Rapid Synthesis of Asymmetric Alkyl- and Aryl-2,9-Disubstituted 1,10-Phenanthrolines. *Tetrahedron Lett.* **2011**, *52*, 3072−3074.
(29) *SADABS Area-Detector Absporption Correction Program*; Bruker AXS: Madison, WI, 2000.
(30) Altomare, A.; Burla, M. C.; Camalli, M.; Cascarano, G. L.; Giacovazzo, C.; Guagliardi, A.; Moliterni, A. G. G.; Polidori, G.; Spagna, R. *SIR97*: A New Tool for Crystal Structure Determination and Refinement. *J. Appl. Crystallogr.* **1999**, *32*, 115−119.
(31) Sheldrick, G. M. A Short History of *SHELX*. *Acta Crystallogr., Sect. A* **2008**, *64*, 112−122.
(32) Ferrugia, L. J. *WinGX* Suite for Small-Molecule Single-Crystal Crystallography. *J. Appl. Crystallogr.* **1999**, *32*, 837−838.
(33) Nazeeruddin, M. K.; Kay, A.; Rodicio, I.; Humphry-Baker, R.; Mueller, E.; Liska, P.; Vlachopoulos, N.; Graetzel, M. Conversion of Light to Electricity by cis-X_2bis(2,2′-bipyridyl-4,4′-dicarboxylate)-ruthenium(II) Charge-Transfer Sensitizers (X = Cl-, Br-, I-, CN-, and SCN-) on Nanocrystalline Titanium Dioxide Electrodes. *J. Am. Chem. Soc.* **1993**, *115*, 6382−6390.
(34) Bard, A. J. ; Faulkner, L. R. In *Electrochemical Methods: Fundamentals and Applications*, 2nd ed; Wiley: New York, 2001.
(35) Magni, M.; Colombo, A.; Dragonetti, C.; Mussini, P. Steric vs Electronic Effects and Solvent Coordination in the Electrochemistry of Phenanthroline-Based Copper Complexes. *Electrochim. Acta* **2014**, DOI: 10.1016/j.electacta.2014.07.086.
(36) Everly, R. M.; McMillin, D. R. Reinvestigation of the Absorbing and Emitting Charge-Transfer Excited States of $[Cu(NN)_2]^+$ Systems. *J. Phys. Chem.* **1991**, *95*, 9071−9075.
(37) Koumura, N.; Wang, Z.-S.; Mori, S.; Miyashita, M.; Suzuki, E.; Hara, K. Alkyl-Functionalized Organic Dyes for Efficient Molecular Photovoltaics. *J. Am. Chem. Soc.* **2006**, *128*, 14256−14257.
(38) Boaretto, R.; Busatto, E.; Carli, S.; Fracasso, S.; Caramori, S.; Bignozzi, C. A. Process for the Synthesis of Precursor Complexes of Titanium Dioxide Sensitization Dyes Based on Ruthenium Polypyridine Complexes. PCT Intl. Appl. WO 2012073268 A1, 2012.
(39) Cazzanti, S.; Caramori, S.; Argazzi, R.; Elliott, C. M.; Bignozzi, C. A. Efficient Non-Corrosive Electron-Transfer Mediator Mixtures for Dye-Sensitized Solar Cells. *J. Am. Chem. Soc.* **2006**, *128*, 9996−9997.
(40) Martineau, D.; Beley, M.; Gros, P. C.; Cazzanti, S.; Caramori, S.; Bignozzi, C. A. Tuning of Ruthenium Complex Properties Using Pyrrole- and Pyrrolidine-Containing Polypyridine Ligands. *Inorg. Chem.* **2007**, *46*, 2272−2277.
(41) Grabulosa, A.; Beley, M.; Gros, P. C.; Cazzanti, S.; Caramori, S.; Bignozzi, C. A. Homoleptic Ruthenium Complex Bearing Dissymmetrical 4-carboxy-4′ -pyrrolo-2,2-bipyridine for Efficient Sensitization of TiO_2 in Solar Cells. *Inorg. Chem.* **2009**, *48*, 8030−8036.
(42) Caramori, S.; Husson, J.; Beley, M.; Bignozzi, C. A.; Argazzi, R.; Gros, P. C. Combination of Cobalt and Iron Polypyridine Complexes for Improving the Charge Separation and Collection in Ru-(terpyridine)$_2$- Sensitised Solar Cells. *Chem.—Eur. J.* **2010**, *16*, 2611−2618.
(43) Boschloo, G.; Haggman, L.; Hagfeldt, A. Quantification of the Effect of 4-*tert*-Butylpyridine Addition to I^-/I_3^- Redox Electrolytes in Dye-Sensitized Nanostructured TiO_2 Solar Cells. *J. Phys. Chem. B* **2006**, *110*, 13144−13150.
(44) Kusama, H.; Konishi, Y.; Sugihara, H.; Arakawa, H. Influence of Alkylpyridine Additives in Electrolyte Solution on the Performance of Dye-Sensitized Solar Cell. *Sol. Energy Mater. Sol. Cells* **2003**, *80*, 167−179.
(45) Abbotto, A.; Coluccini, C.; Dell'Orto, E.; Manfredi, N.; Trifiletti, V.; Salamone, M.; Ruffo, R.; Acciarri, M.; Colombo, A.; Dragonetti, C.; Ordanini, S.; Roberto, D.; Valore, A. Thiocyanate-Free Cyclometalated Ruthenium Sensitizers for Solar Cells Based on Heteroaromatic-Substituted 2-arylpyridines. *Dalton Trans.* **2012**, *41*, 11731−11738.
(46) Dragonetti, C.; Valore, A.; Colombo, A.; Magni, M.; Mussini, P.; Roberto, D.; Ugo, R.; Valsecchi, A.; Trifiletti, V.; Manfredi, N.; Abbotto, A. Ruthenium Oxyquinolate Complexes for Dye-Sensitized Solar Cells. *Inorg. Chim. Acta* **2013**, *405*, 98−104.
(47) Dragonetti, C.; Colombo, A.; Magni, M.; Mussini, P.; Nisic, F.; Roberto, D.; Ugo, R.; Valore, A.; Valsecchi, A.; Salvatori, P.; Lobello, M. G.; De Angelis, F. Thiocyanate-Free Ruthenium(II) Sensitizer with a Pyrid-2-yltetrazolate Ligand for Dye-Sensitized Solar Cells. *Inorg. Chem.* **2013**, *52*, 10723−10725.